Journal of the Korean Vacuum Society
Vol. 2, No. 2, June 1993, pp. 171-180

〈연구논문〉

XPD Analysis on the Cleaved GaAs(110) Surface

D. H. Lee*, J. Chung and S.-J. Oh**

Department of Physics, Seoul National University, Seoul 151-742, Korea

(Received May 19, 1993)

절개된 GaAs(110) 면의 XPD 분석

이덕형* · 정재관 · 오세정**

서울대학교 자연과학대학 물리학과

(1993년 5월 19일 접수)

Abstract – X-ray photoelectron diffraction (XPD) is used to characterize the crystallographically cleaved GaAs(110) surface. By using polar and azimuthal scans of the usual angle-resolved x-ray photoelectron spectroscopy, we get the reconstruction geometry of the clean GaAs(110) surface from the intensity ratio of Ga 3*d* and As 3*d* core-level peaks. The reconstruction parameters are determined by fitting the diffraction pattern with the single scattering cluster (SSC) model, and the results show similar tendencies to those obtained by other techniques.

요 약 – X-선 광전자 분광법(XPD)을 이용하여 GaAs(110) 절개면의 결정구조를 이해하였다. 각분해 X-선 분광법으로 GaAs(110) 면의 내각준위 Ga 및 As 3*d*의 스펙트럼을 얻어, 이 내각 준위의 세기 비율(intensity ratio)의 방위각과 편각에 따른 변화를 SSC(Single Scattering Cluster) 모델에서 얻은 회절패턴으로 곡선분석(fitting)하여 절개면의 재구성 구조(reconstruction geometry)를 얻었다. 이 절개면의 재구성된 값은 다른 실험의 결과와 비슷하였다.

1. Introduction

The x-ray photoelectron peak intensity of a core level from a single crystal surface generally shows a large angular variation both along the polar and azimuthal take-off angle. It is known to be caused by the diffraction of outgoing photoelectrons by neighboring atoms, so called x-ray photoelectron diffraction (XPD) effect[1, 2]. Since XPD process mainly consists of the electron scattering with atoms, the general multiple scattering theory which has been developed, for example, for the analysis of low energy electron diffraction (LEED) can give a complete understanding for this process.

According to the multiple scattering theory[3], the scattering amplitude falls off with the order of $(kR)^{-n}$ for the nth scattering where k is the wavevector of the outgoing electron and R is the distance between the adjacent scatterers. Therefore, the diffraction of electrons with kinetic energy higher than ~500 eV ($kR \gg 1$) can usually be calculated considering only the single scattering event without serious errors. But the scattered waves of electrons in the high energy range are strongly forward directional and backscattering is very weak,

*Present address: Samsung Electronics Semiconductor Business, Memory Division Advanced Technology Center, Basic Research Department, P.O. Box 37, Suwon, Korea

**Author to whom all correspondences should be addressed

thus they cannot be used as an external probe except for the very grazing incidence as for reflection high energy electron diffraction (RHEED). That is the reason why LEED must use only low energy electrons below ~300 eV in spite of the difficulty of the full multiple scattering calculation. On the other hand, photoelectrons ejected from atoms below the topmost layer(s) can undergo collisions on their way out to the vacuum, and this forward directional scattering property of high energy electrons can be utilized to analyze the XPD pattern simply by the single scattering theory, which is a big advantage over the LEED. Also XPD pattern shows up even in the absence of any long range order, which is necessary for the LEED study. But the large inelastic mean free path of outgoing electrons (typically 20 Å for the kinetic energy of 1000 eV) makes XPD less surface sensitive than LEED or RHEED.

As a model calculation for the analysis of XPD, the single scattering cluster (SSC) model has been developed by Fadley *et al.*[1] over the prior theoretical backgrounds of *ab initio* formulations[4-7]. In spite that many questions have been raised about the assumptions of this model such as the "small atom" approximation of the multiple scattering effect[9-11], it has been successfully applied to many adsorbate systems and proved to be a quite good approximation for most cases[11-20]. The discrepancy of SSC calculation with the experiment, however, has been often found for the highly symmetric directions where the one dimensional atomic chain may be formed. In those directions, experimentally measured XPS intensities are considerably less than the calculated values. Recently, Xu *et al.* have shown by their multiple scattering calculation for one dimensional atomic chain that successive scatterings with several atoms along the same direction reduce XPS intensity significantly by the "defocusing" effect[10]. The experimental tests for this effect also have been made for the XPD of plasmon loss peak which is composed of the electrons with deeper depth distribution of emitting positions than that of the main peak with no loss, thus confirming the prediction that intensity enhancement ratio is less for those directions where several atoms successively appear[21, 22].

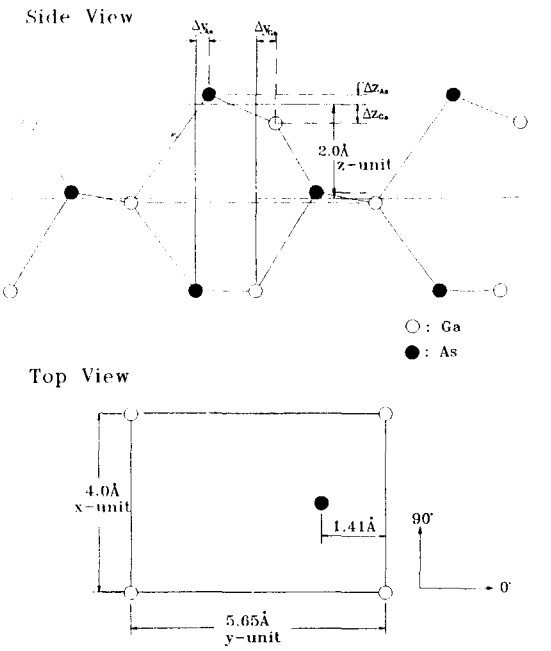

Fig. 1. Reconstruction geometry of the GaAs(110) surface. The angles indicate the reference directions used in the experiment.

The angular variation of XPS intensity of clean GaAs surfaces has been reported[23, 24] but the theoretical calculation of XPD has been reported only for the (100) surface recently[19], and not for the (110) surface yet. Since GaAs single crystal is well cleaved along the [110] direction, many investigations about surface reconstructions and adsorptions phenomena have been performed on the (110) surface[25-32]. Hence the model calculation of XPD for clean (110) surface is necessary for further XPD researches on the adsorbate systems of GaAs such as oxygen or metals. The surface atoms of clean GaAs(110) surface are known to reconstruct to lower the total surface energy, and the reconstructed geometry determined by experiments (dynamical LEED)[25, 31, 32] and theoretical calculations (cluster calculation[33, 34], total energy minimization[35, 36]) shows general agreement. According to these results, gallium atoms of topmost layer moves to a lower position to make three bonding planar and the arsenic atom moves to slightly upper position with two dangling bonds, as shown in Fig.

1. In this work, we performed the azimuthal and polar scans of XPS intensities of Ga and As core-levels on the GaAs(110) surface which was obtained by the cleavage in the UHV (Ultra High Vacuum) chamber, and compared the data with the XPD patterns calculated by the SSC model. We obtain the relaxation parameters from the best fit, and the reason for some discrepancy between experiment and theory is discussed in terms of the defocusing effect.

2. Single Scattering Cluster Theory

XPD phenomenon is a consequence of the interference between the primary wave excited from a given site and the secondary waves scattered by atoms at other sites. The primary spherical wave intensity has an angular dependence given by [37]

$$L(\theta_k)=1+\frac{1}{2}\beta(3\cos^2\theta_k-1) \quad (1)$$

where β is a constant for a given subshell of a given atom and θ_k is the angle between the photon polarization vector and the outgoing wavevector k. For the simple case of spherically symmetric s initial state where $\beta=2$ for all atoms, the angular dependence of the primary wave amplitude is proportional to $\varepsilon\cdot k$.

In most cases of a few Å lattice constant, the following two important approximations can be made without serious errors.

1. The differential cross section for excitations can be calculated by using a plane wave final state exp ($ik\cdot r$) and thus has an angular depencence of k for emission from a spherically symmetric subshell.

2. The primary photoelectron wave can be approximated by a plane wave at the time it reaches the scatterers (the "small-atom" approximation).

The inelastic scattering effect is included as an isotropic attenuation of intensity with the inelastic mean free path (IMFP) λ and the thermal vibration is introduced via the Debye-Waller factor, $W_j=\exp(-2k^2(1-\cos\theta_j)U_j^2)$, where U_j^2 is the one-dimensional mean-squared displacement to the jth atom with

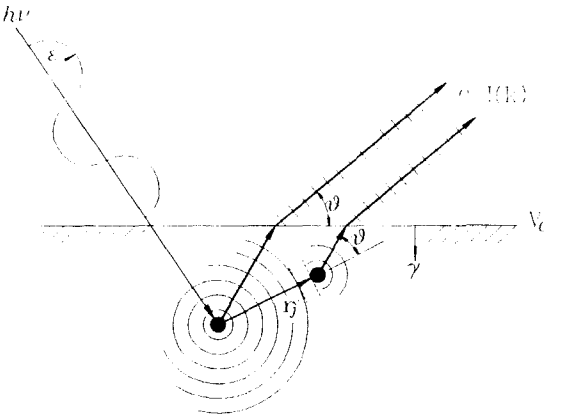

Fig. 2. Schematic diagram of the photoelectron diffraction process.

respect to the emitter. For the unpolarized x-ray source, the intensity from the s state along the k direction considering only single scattering events is therefore given by

$$I(k)\propto\int|\varepsilon\cdot k\exp(-\gamma L)+\sum_j\frac{\varepsilon\cdot r_j}{r_j}f_j(\theta_j)W_j\exp(-\gamma L_j)\exp[ikr_j(1-\cos\theta_j)]|^2d\varepsilon+\sum_j\int(\varepsilon\cdot r_j)^2\frac{|f_j(\theta_j)|^2}{r_j^2}(1-W_j^2)\exp(-2\gamma L_j)d\varepsilon \quad (2)$$

where the integration with respect to ε is over 360° in the plane of polarization of the incident x-rays. The variables included in equation 2 are illustrated in Fig. 2 and defined as follows:

γ : $1/2\lambda$

L : relevant path length from the emitter to the surface

L_j : path length from the emitter to the jth scatterer toward the surface

$f_j(\theta_j)=|f_j(\theta_j)|\exp[i\Psi_j(\theta_j)]$: scattering factor with a phase shift

t_j : position of the jth scatterer

θ_j : scattering angle

The second term in equation 2 is included to correct for the unphysical inclusion of the Debye-Waller attenuation on the same atom in the first term.

The scattering factor $j_l(E,\ \theta_j)$ is calculated by the following relation with the phase shifts δ_l's of the

lth partial wave[38].

$$f(E,\theta)=\sum \frac{1}{k}(2l+1)\sin(\delta_l)\exp(i\delta_l)P_l(\cos\theta)$$
$$=|f(\theta)|\exp[i\Psi(\theta)] \quad (3)$$

where $P_l(\cos\theta)$ is the lth Legendre function. Because of the strong forward peaking of $f_j(\theta_j)$ in the XPS energy range, the approximation $\cos(k, r_j)=\cos(r_j, r_i)=1$ would give no noticeable differences in comparison with the exact calculation. With those approximations, equation 2 can be simplified as

$$I(k)\propto|\exp(-\gamma L)\sin(\theta_k)$$
$$+\sum_j I_j W_j \exp i[kr_j(1-\cos\theta_j)+\Psi_j(\theta_j)]|^2$$
$$+\sum_j I_j^2(1-W_j) \quad (4)$$

where $I_j=|f_j(\theta_j)|\sin(\theta_{r_j})\exp(-\gamma L_j)/r_j$ and θ_k or θ_{r_j} are the angles between the polarization plane and k or r_j, respectively. Equation 4 can be applied for any initial state, since the values of θ_k in equation 1 become important only in the narrow range around the fixed angle between the direction of the analyzer and the x-ray incidence.

The direction of the photoelectrons can change slightly due to the refraction through the surface as

$$\tan\theta=\frac{(\sin\theta'-V_o E_k)^{1/2}}{\cos\theta'} \quad (5)$$

where V_o is the inner potential, E_k is the kinetic energy of the electron inside the solid, and θ' and θ and the polar angles with respect to the surface inside or outside of the solid, respectively. This effect is small, and will be neglected in the subsequent analyses.

3. Experiment

The techniques employed in this investigation are XPS and ultraviolet photoemission spectroscopy (UPS). All the spectra were collected by the VSW ESCA/AUGER system at Seoul National University. Photon source for XPS was Al-Kα ($h\nu=1486.6$ eV) and UPS sources were He I ($h\nu=21.2$ eV) and He II ($h\nu=40.8$ eV). Concentric hemispherical analyzer (CHA) was used to measure the photoemitted electron energy distribution with pass energies of 22 eV and 44 eV of XPS and 10 eV for UPS. High pass energies were used to increase the intensity rather than to get the high resolution.

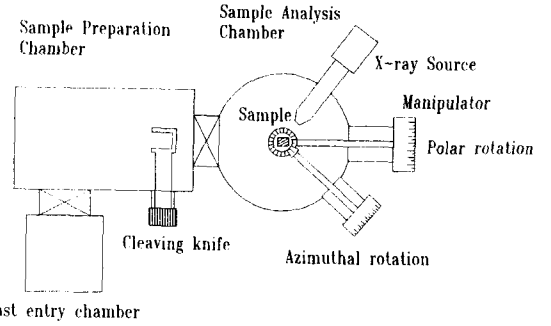

Fig. 3. Schematic picture of the spectrometer and the rotation geometry (CHA points upward).

With the angle between directions of the x-ray incidence and the electron detection fixed as 60° by the construction of the experimental chamber, the samples were rotated about the azimuthal and polar axes for the take-off angle scan. Polar rotation was made by the direct rotation of the sample manipulator axis at the end of which sample holder is mounted. For the azimuthal rotation, gears were made both around the sample holder and the axis of the external rotary feedthrough, which were engaged to each other to make the sample rotation possible by rotating the external rotary feedthrough. The structure of the spectrometer and the rotating geometry are illustrated in Fig. 3. The angular resolution of rotators was $\Delta\theta\sim0.1°$ for the polar scan and $\Delta\phi\sim0.5°$ for the azimuthal scan where the backlash gives somewhat larger error. The acceptance angle of the analyzer was estimated less than 3° from the entrance aperture radius and the distance from the sample. We obtained the experimental results of the polar scan at the azimuthal angle $\phi=180°$, 235° and the azimuthal scan at the polar angle $\theta=35°$, 60°. The reason for these choices of angles is that strong diffraction effects due to the forward scattering are expected at there angles. For example, the zinc-blende structure of GaAs has the Ga-As bonding direction at $\theta\sim35°$ and $\phi=180°$. If the electron take-off angle accords with the bonding direction or other forward atom's

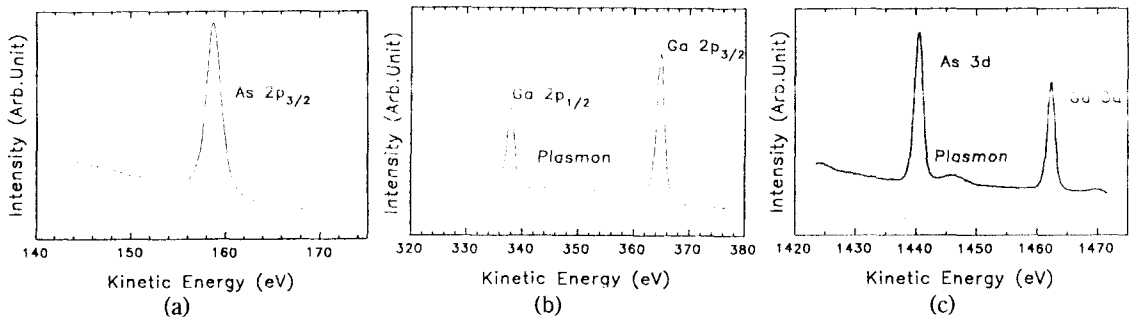

Fig. 4. XPS spectra of the cleaved GaAs(110) surface, (a) As $2p_{3/2}$ (b) Ga $2p$ (c) As $3d$ and Ga $3d$ peaks.

direction, we expect to see the large peaks of diffraction pattern.

The sample used in this experiment was Si-doped n-GaAs with the doping concentration of $4\sim6\times10^{18}/cm^3$. The clean GaAs(110) surfaces were obtained by cleaving a rectangulary bar with the cross section of $3\times5\,mm^2$ in the ultra high vacuum of the pressure less than 5×10^{-9} mbar.

4. Results and Discussions

The As, Ga $2p$ and As, Ga $3d$ spectra of the clean GaAs(110) surface cleaved inside the UHV spectrometer are illustrated in Fig. 4. The As $2p$ and Ga $2p$ raw spectra in Fig. 4(a) and 4(b) have background increasing with the electron kinetic energy due to the analyzer transmission function with the electron kinetic energy, which makes the curve fitting routine a little difficult. Approximating the transmission function as E^{-1}, the corrected spectra show almost flat backgrounds, which were used in our analysis.

The surface cleanliness cannot be sufficiently checked by only XPS because carbon or oxygen, the main contaminating elements, have very little cross sections of the valence state in the x-ray photon energy range. But their cross sections at the photon energy of He II ($h\nu=40.8$ eV) are several ten times larger than those of Ga and As valence state electrons and also this photon energy gives high surface sensitivity[39]. Hence UPS with the He source can check the surface cleanliness very sensitively. In Fig. 5, we show UPS spectra of the clean GaAs(110) surface, where no features from the contaminants (e.g. hydrocarbon at 7~8 eV) are

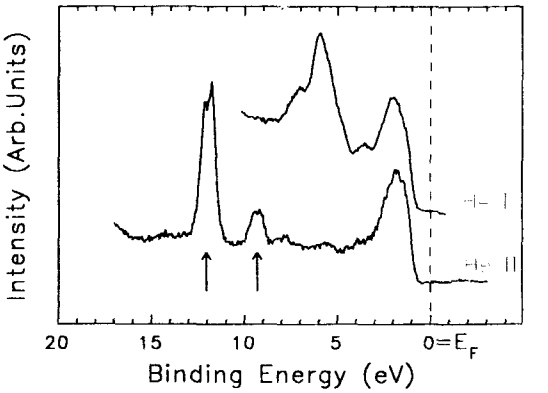

Fig. 5. UPS spectra of the cleaved GaAs(110) surface with He I and He II sources (Two arrowed peaks in the case of He II source are the satellites of Ga $3d$ level due to the He II source satellites).

observed.

The core-level spectra shown in Fig. 4 are fitted by the curve fitting routine. The parameters determined by the least square fitting are given in Table 1. For the maximization of intensity, the analyzer pass energies were chosen to have somewhat large values of 44 eV for the $3d$ spectra and 22 eV for the $2p$ spectra, which inevitably give poor resolution. Since the main aim of this work was not to resolve the various chemical states but to measure the peak intensities accurately, somewhat poor resolution condition was inevitable. With that resolution, the spin-orbit splitting of the $3d$ peaks and the surface shifted components (0.28 eV for Ga $3d$ and -0.37 eV for As $3d$)[25] were not fully resolved.

The atomic wavefunctions used for the muffin-tin

Table 1. Parameters of the photoemission core-level peaks determined by the least square fitting procedure. The binding energies were determined from the following equation. $E_{bin}=h\nu-E_{kin}-W$ where $h\nu=1486.6$ eV for Al-Kα and the instrumental work function $W=4.8$ eV.

Atomic level	As $2p_{3/2}$	Ga $2p_{3/2}$	As $3d$	Ga $3d$
Kinetic energy (eV)	158.6	364.5	1440.7	1462.8
Binding energy (eV)	1323.2	1117.3	41.1	19.0
Lorentzian HWHM (eV)	1.2(± 0.05)	1.1(± 0.05)	0.6(± 0.05)	0.6(± 0.05)
Gaussian HWHM (eV)	1.1(± 0.05)	1.0(± 0.1)	1.0(± 0.05)	1.0(± 0.05)

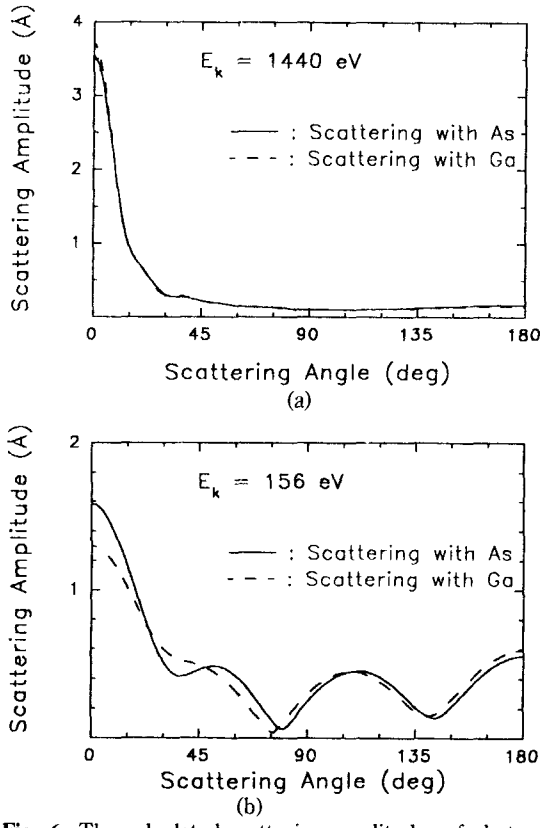

Fig. 6. The calculated scattering amplitudes of photoelectrons, (a) As $3d$ ($E_{kin}=1440$ eV) (b) As $2p$ ($E_{kin}=156$ eV).

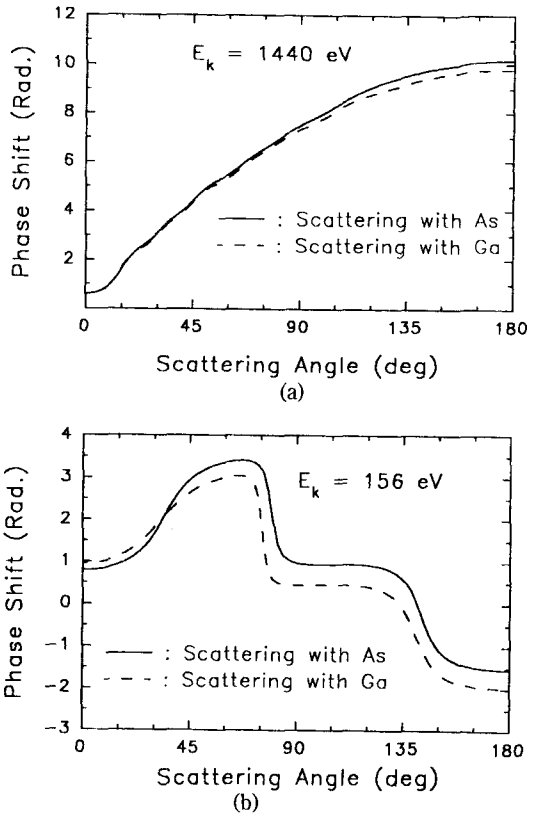

Fig. 7. The calculated phase shifts of photoelectrons, (a) As $3d$ ($E_{kin}=1440$ eV) (b) As $2p$ ($E_{kin}=156$ eV).

potential to calculate the electron scattering factor $f_j(\theta_j)$ were Herman-Skillman wavefunction[40] which were renormalized as if they were all within the muffin-tin radius with the valence electron wavefunctions being uniform. The scattering factors of each species were calculated using the computer program made by Pendry for LEED analysis[38]. The scattering amplitude and the phase shift of Ga and As atoms for the photoelectrons from As $3d$ ($E_k\simeq 1440$ eV) and As $2p$ ($E_k\simeq 156$ eV) core levels are illustrated in Figs. 6 and 7 respectively. It can be seen that the forward scattering is dominant for the $3d$ peak but it is not the case for the $2p$ peak which has smaller kinetic energy. Since the scattering factors depend only on the electron energy and the scatterer, those from the Ga $3d$ level ($E_k=1465$ eV) are quite similar to the results for the As $3d$ level. The inelastic mean free path

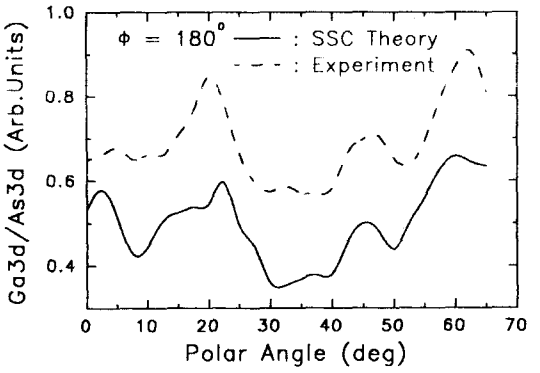

Fig. 8. Polar XPD patterns at the azimuthal angle of 180°.

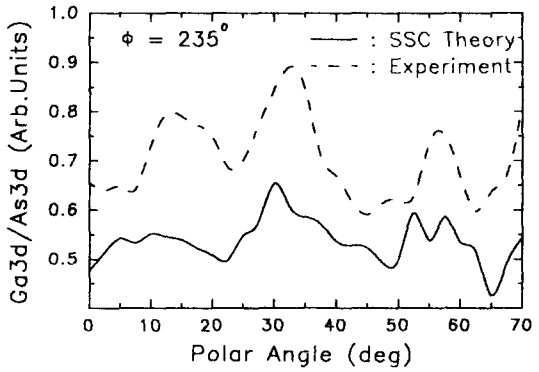

Fig. 9. Polar XPD patterns at the azimuthal angle of 235°.

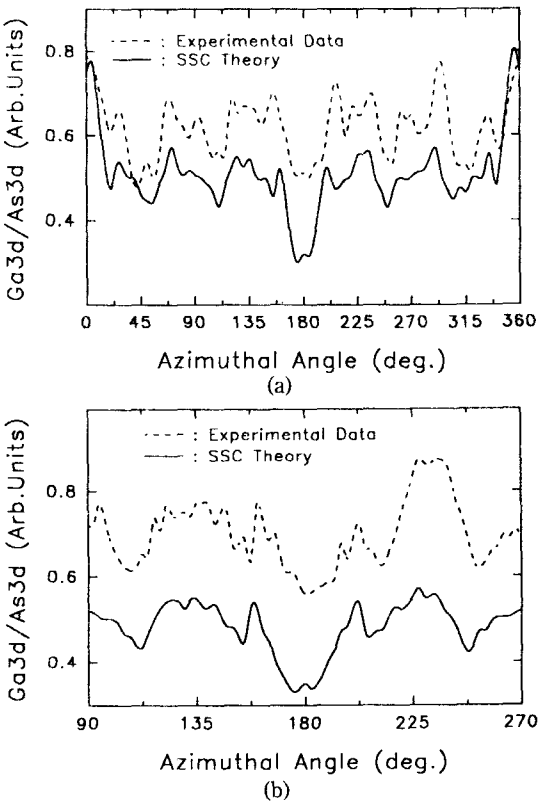

Fig. 10. Azimuthal XPD patterns at the polar angle of 35°, (a) angle increment=5°, (b) angle increment=2.5° (fine scan).

for the attenuation was fixed as in Ref.[23] for both As 3*d* and Ga 3*d* levels by a rough estimation from the universal equation by Seah and Dench [41]. The cluster size used for the SSC model calculation was 11×9×7 (The unit for each direction is marked in Fig. 1). As mentioned before, the surface refraction effect was ignored in our analysis since the values of the angle change evaluated from equation 5 are less than 0.5°, which is quite smaller than the angle increments used in this experiment.

The XPD patterns of polar and azimuthal scans for Ga and As 3*d* core-levels are shown in Figs. 8, 9 and 10, where they are compared with the results of the SSC calculations. Since it was impossible to evaluate the photon flux change along the scanning angle, the absolute intensity variation for each peak could not be obtained. Hence we show in these figures only the ratio of peak intensities. We can see from these figures that a global agreement between experimental XPD patterns and computer simulation results from the SSC calculation is found for both polar and azimuthal scans. The reference azimuthal angle direction is marked in Fig. 1. The small discrepancies between experimental data and SSC calculations that can be found in these figures are considered to have a few origins. First, errors from the poor angular resolution for the azimuthal scan would give uniform noise over all measured angles. Errors can also be included in the calculation of scattering factors by some arbitrariness in fixing the muffin-tin radius and in the assumption that the inelastic effect is isotropic.

However, the main discrepancy between the SSC theory and the experiment seems to be caused by the multiple scattering effect. As mentioned in the previous section, the multiple scattering in general

need not be considered in high energy electron diffraction, but it becomes important in the case that several atoms appear successively along the direction to which electron propagates. It has been recently found[10, 20, 21] that scatterings with successive atoms reduce the XPS intensity significantly by "defocusing" effect, whereas the scattering with a single atom focuses the electron wave. The intensities of the plasmon loss peak for such directions are expected to be more reduced than those of no loss peak, because the depth distribution of the electrons which suffer any inelastic scattering would be deeper than that of electrons with no loss, thus the loss peak would include more defocusing effect. Since SSC calculation does not include the defocusing effect, the calculated intensity would be much larger than the experimental intensity for those directions.

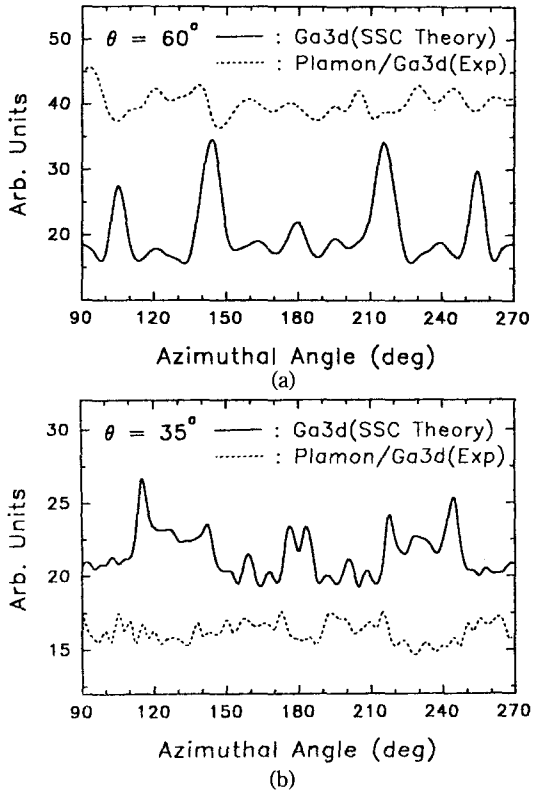

Fig. 11. Azimuthal patterns of the intensity ratio of the Ga 3*d* plasmon loss peak and the Ga 3*d* XPD patterns calculated by the SSC theory. (a) polar angle=60°, (b) polar angle=35°. It is shown that the plasmon loss peak intensity ratios are slightly less for the directions of (a) 105, 145, 215, 255° and (b) 180° where the calculated Ga 3*d* peak intensities are large.

The GaAs structure has no exact one-dimensional chain, but along several directions the chain-like arrangements with small positional deviations are found. For those directions the SSC calculation would predict much larger peak intensity than actually observed, and the experimental intensity ratio of the plasmon loss peak relative to the main peak would be smaller than those for other directions. In Figs. 11(a) and 11(b), the calculated Ga intensity patterns and the experimental loss peak intensity ratio patterns are compared with each other. In both figures, the loss peak intensity ratios are shown to be smaller at the angles where the calculated Ga intensity has a large peak, implying that the defocusing effect is included for those directions.

Determination of the clean surface reconstruction was tried by modulating the first and second layer atomic positions in the SSC calculation and searching for the position with minimum standard deviations from the experimental data, the results of which are given in Table 2 and compared with other results[22, 31, 36]. But the values evaluated in this work may have a larger error because the surface contribution in this energy range is as small

Table 2. Reconstruction geometry of the GaAs(110) surface (arrows indicate the directions of the displacements)

Δz_{As}(Å)	Δz_{Ga}(Å)	Δy_{As}(Å)	Δy_{Ga}(Å)	ω(deg)	Reference
0.19 (↑)	0.46 (↓)	0.19 (→)	0.35 (→)	27.3	[36]
0.144 (↑)	0.506 (↓)	0.33 (→)	0.48 (→)	27	[22]
0.176 (↑)	0.510 (↓)	0.22 (→)	0.34 (→)	27	[31]
0.2 (↑)	0.5 (↓)	0.4 (→)	0.4 (→)	24	This work

as 10% defocusing effect mentioned above might give larger changes on the patterns than does the variation of surface atomic positions. Nevertheless, the tendency of the reconstruction and the twist angle of 24° are sufficient to confirm the well known 27° tilted model and to discard the 7° model proposed some time ago[31, 35, 36].

5. Summary

Our results of the XPD analysis for the clean GaAs(110) surface can be summarized as follows:

1. The XPS intensity of each element (Ga or As) for the clean surface shows a large variation with both polar and azimuthal take-off angle changes. The SSC model calculation for the photoelectron diffraction effect provides the patterns quite similar to the experiments.

2. The main discrepancy between experiments and the result of the SSC calculation is due to the "defocusing effect" along the directions of the chain-like arrangement, which was confirmed by the reduction of the plasmon loss peak intensities along those angles.

3. The reconstruction geometry evaluated from the XPD analysis shows a similar tendency to those measured by other techniques.

Acknowledgement

This work was supported by the grant from the Korean Science and Engineering Foundation.

Reference

1. C. S. Fadley, *Prog. Surf. Sci.* **16**, 275 (1984).
2. S. A. Chambers, *Adv. in Phys.* **40**, 357 (1991).
3. T. Fuzikawa, *J. Phys. Society of Japan* **50**, 1321 (1981).
4. A. Liebsch, *Phys. Rev. Lett.* **32**, 1203 (1974).
5. A. Liebsch, *Phys. Rev.* **13**, 544 (1976).
6. P. A. Lee, *Phys. Rev.* **13**, 5261 (1976).
7. C. H. Li, A. R. Lubinsky and S. Y. Tong, *Phys. Rev.* **B17**, 3178 (1978).
8. J. J. Barton and D. A. Shirley, *Phys. Rev.* **B32**, 1906 (1985).
9. S. Y. Tong, T. C. Poon, and D. R. Snider, *Phys. Rev.* **B32**, 2096 (1985).
10. M.-L. Xu, J. J. Barton and M. A. Van Hove, *Phys. Rev.* **B39**, 8275 (1989).
11. S. Kono, S. M. Goldberg, N. F. T. Hall and C. S. Fadley, *Phys. Rev. Lett.* **41**, 1831 (1978); *Phys. Rev.* **B22**, 6085 (1980).
12. L.-G. Petersson, S. Kono, N. F. T. Hall, C. S. Fadley and J. B. Pendry, *Phys. Rev. Lett.* **42**, 1545 (1979).
13. P. J. Orders, R. E. Conelly, N. F. Hall and C. S. Fadley, *Phys. Rev.* **B24**, 6163 (1981).
14. E. L. Bullock and C. S. Fadley, *Phys. Rev.* **B31**, 1212 (1985).
15. D. A. Wesner, F. P. Coenen and H. P. Bonzel, *Phys. Rev. Lett.* **60**, 1045 (1988).
16. R. S. Saiki, G. S. Herman, M. Yamada, J. Osterwalder and C. S. Fadley, *Phys. Rev. Lett.* **63**, 283 (1989).
17. S. A. Chambers and V. A. Loebs, *Phys. Rev. Lett.* **63**, 640 (1989).
18. R. Baptist, S. Ferrer, G. Grenet and H. C. Poon, *Phys. Rev. Lett.* **64**, 311 (1990).
19. S. A. Chambers, *Phys. Rev.* **B42**, 10865 (1990).
20. J. Osterwalder, T. Greber, S. Hüfner and L. Schlapbach, *Phys. Rev.* **B41**, 12495 (1990).
21. G. S. Herman and C. S. Fadley, *Phys. Rev.* **B43**, 6792 (1991).
22. R. J. Meyer, C. B. Duke, A. Paton, A. Kahn, E. So, J. L. Yeh and P. Mark, *Phys. Rev.* **B19**, 5194 (1979).
23. P. Alnot, F. Wyczisk and A. Friederich, *Surf. Sci.* **162**, 708 (1985).
24. S. Evans and M. D. Scott, *Surface Interface Anal.* **3**, 269 (1981).
25. D. E. Eastman, T.-C. Chiang, P. Heimann and F. J. Himpsel, *Phys. Rev. Lett.* **45**, 1045 (1981).
26. J. A. Stroscio, R. M. Feenstra and A. P. Fein, *Phys. Rev. Lett.* **58**, 1668 (1987).
27. J. A. Stroscio, R. M. Feenstra, and A. P. Fein, *Phys. Rev.* **B36**, 7718 (1987).
22. K. A. Bertness, J.-J. Yeh, D. J. Friedman, P. H. Mahowald, A. K. Wahi, T. Kendelewicz, I. Lindau and W. E. Spicer, *Phys. Rev.* **B38**, 5406 (1988).
29. P. Mårtensson and R. M. Feenstra, *Phys. Rev.* **B39**, 7744 (1989).
30. A. B. McLean and F. J. Himpsel, *Phys. Rev.* **B40**, 8425 (1989).
31. S. Y. Tong and W. N. Mei, *J. Vac. Sci. Technol.* **B2**, 393 (1984).
32. C. B. Duke, S. L. Richardson, A. Paton and A. Kahn, *Surface Sci.* **127**, L135 (1983).

33. J. J. Barton, W. A. Goddard and T. C. McGill, *J. Vac. Sci. Technol.* **16**, 1178 (1979).
34. J. J. Barton, C. A. Swarts, William A. Goddard and T. C. McGill, *J. Vac. Sci. Technol.* **17**, 164 (1980).
35. D. J. Chadi, *Phys. Rev. Lett.* **41**, 1062 (1978).
36. D. J. Chadi, *Phys. Rev.* **B19**, 2074 (1979).
37. E. E. Koch, *Handbook on synchrotron radiation,* North-Holland Publishing Company (1983).
38. J. B. Pendry, *Low Energy Electron Diffraction,* Academic Press, London (1974).
39. J. J. Yeh and I. Lindau, *Atomic data and Nuclear data tables* **32**, 1 (1985).
40. F. Herman and S. Skillman, *Stomic Structure Calculation,* Prentice-Hall, Inc., New Jersey (1983).
41. M. P. Seah and D. P. Dench, *Surf. Int. Anal.* **1**, 2 (1979).